Organic & Biomolecular Chemistry

Plasmid DNA delivery using arginine-rich cell-penetrating L/D-peptides containing α-aminoisobutyric acids

Journal:	*Organic & Biomolecular Chemistry*
Manuscript ID	OB-ART-04-2025-000627.R1
Article Type:	Paper
Date Submitted by the Author:	28-Apr-2025
Complete List of Authors:	Umeno, Tomohiro; Kyoto Prefectural University of Medicine Takemoto, Hiroyasu; Kyoto Prefectural University of Medicine Oba, Makoto; Kyoto Prefectural University of Medicine, Department of Molecular Medicinal Sciences

ARTICLE

Plasmid DNA delivery using arginine-rich cell-penetrating L/D-peptides containing α-aminoisobutyric acids

Received 00th January 20xx,
Accepted 00th January 20xx

DOI: 10.1039/x0xx00000x

Tomohiro Umeno,*[a] Hiroyasu Takemoto[a] and Makoto Oba*[a]

The relationship between intracellular uptake efficacy and the folding behavior of arginine-rich cell-penetrating L/D-peptides with α,α-disubstituted α-amino acids in plasmid DNA (pDNA) delivery was examined. Nano-sized complexes formed from pDNA and L/D-peptides efficiently traversed the cell membrane regardless of the peptide conformation. This finding represents a significant deviation from previously reported covalent cargo delivery methods using cell penetrating peptides with L- and D-amino acids.

Introduction

Cell-penetrating peptide (CPP) foldamers are powerful tools for delivering bioactive and membrane-impermeable molecules, such as nucleic acids, proteins, drugs, and imaging agents, into cells.[1] Cationic CPPs containing arginine (Arg) residues represent a typical class of CPPs, as their positively charged side chains interact electrostatically with the anionic cell membrane, thereby facilitating intracellular uptake.[2] Although there is growing interest in CPPs, extensive efforts to enhance their membrane permeability and further optimization are still required for clinical applications.[3] To date, no CPPs or CPP cargo formulations have been approved by the Food and Drug Administration (FDA), primarily because of instability in biological environments.

To address these limitations, various chemical modifications have been applied to the peptides. One effective approach to improve the stability and activity of CPPs is the incorporation of α,α-disubstituted α-amino acids (dAAs), which possess additional alkyl substituents at the α-position of the α-amino acid.[4] The distinctive properties of dAAs, including their high hydrophobicity, chemical stability, and ability to stabilize peptide secondary structures, contribute to the improved cell membrane permeability of CPPs. Substituting L-isomers with D-isomers is another effective approach for enhancing CPP stability.[5] D-Isomers are generally not recognized by proteases, which helps to prevent the enzymatic degradation of peptides and allows prolonged intracellular delivery of cargo. However, some studies have shown that D-peptides exhibit lower cell membrane permeability compared to their L-isomer counterparts owing to their destabilized conformations.[6]

Demizu et al. investigated dual-modified peptide foldamers composed of dAAs and D-amino acids, functioning as CPPs and as antimicrobial peptides.[7] In this study, the incorporation of D-amino acids into Arg-rich peptide foldamers containing dAAs exhibited both advantageous and detrimental effects on their cell-penetrating ability. Fluorescence-labeled D-CPP, in which all Arg residues are in the D-form, demonstrated more efficient cellular penetration than its L-isomer counterpart (L-CPP).[7a] However, for the delivery of phosphorodiamidate morpholino oligomers (PMOs), PMO-conjugated D-CPP exhibited similar delivery efficacy as that of L-CPP.[7b] Therefore, the type of cargo appears to be a critical factor in determining whether the L- or D-form is more suitable. Incidentally, heterochiral L/D-CPPs constructed from both L- and D-Arg were inferior to the homochiral L-CPPs and D-CPPs in both cases.

In this study, we focused on the delivery of plasmid DNA (pDNA) through the formation of nanoparticles (NPs) using L-, DL-, LD-, and D-CPPs **1**–**4**, which incorporate Arg and α-aminoisobutyric acid (Aib), the simplest dAA.[8] Positively charged peptides form NPs with negatively charged pDNA through non-covalent interactions, such as electrostatic and hydrogen bonding. Given that both nucleic acids and amino acids are chiral molecules, the formation of NPs may depend on the chiral compatibility between pDNA and peptides, which could influence their efficacy in penetrating cell membranes. Therefore, we aimed to elucidate the effects of structural and conformational differences in CPPs on the formation of NPs with pDNA and their transfection efficiency (Figure 1).

[a] *Graduate School of Medical Science, Kyoto Prefectural University of Medicine, 1–5 Shimogamohangi-cho, Sakyo-ku, Kyoto 606–0823, Japan.*

† Footnotes relating to the title and/or authors should appear here.

Supplementary Information available: [details of any supplementary information available should be included here]. See DOI: 10.1039/x0xx00000x

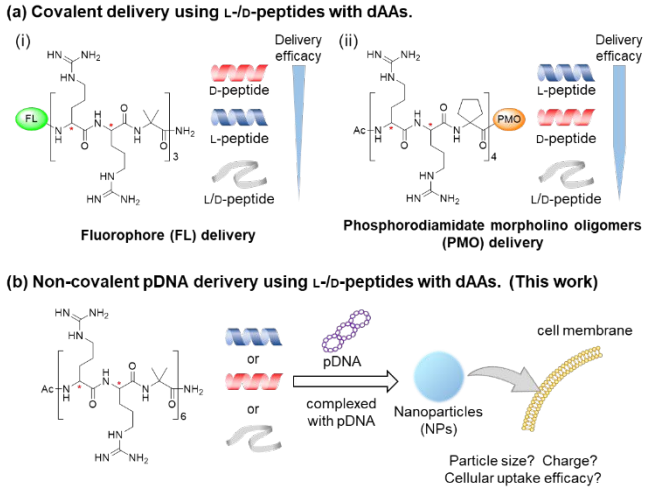

Figure 1. (a) Previously reported covalent cargo delivery using L/D-CPPs with dAAs and (b) the present study.

Results and discussion

Synthesis and characterization of peptides.

We synthesized four peptides **1**–**4** using the Fmoc solid-phase peptide synthesis method (Figure 2a). These peptides are Aib CPP foldamers designed for pDNA delivery following the previously reported procedure from our group.[9] All peptides were purified using HPLC and confirmed by LC-MS. Based on the retention times observed during reverse-phase analytical HPLC, **2** and **3** (t_R = 11.0 min) appeared to be more hydrophilic than **1** and **4** (t_R = 11.7 min). The secondary structures of peptides **1**–**4** were characterized by recording their CD spectra in aqueous solutions at a concentration of 0.05 mM (Figure 2b). Peptide **1**, composed entirely of L-isomers, exhibited a positive maximum at 190 nm and negative maxima around 204 and 225 nm, which correspond to the amide perpendicular π-π*, parallel π-π*, and perpendicular n-π* transitions, respectively.[10] The CD spectrum of **1** suggested a right-handed helical structure of **1** attributed to the presence of Aib as a helical inducer.[7a,9,11] As anticipated, peptide **4**, the enantiomer of **1**, displayed a spectrum that was nearly a mirror image of that of peptide **1**, indicating that it adoption of a left-handed helical structure. In contrast, peptides **2** and **3** did not form the typical single-handed helical structures and exhibited random coil-like CD spectra. The CD spectrum of **3**, with a negative maximum at 199 nm and a positive maximum at 225 nm, was similar to that of nonaarginine (R9), a representative CPP that does not contain dAAs,[12] despite **3** containing six Aibs in its sequence. Additionally, the CD spectra of **3** was completely different from that of Boc-(L-Leu-D-Leu-Aib)$_4$-OMe,[13] which forms a right-handed α-helix, even though the molecular configurations of peptides **3** and Boc-(L-Leu-D-Leu-Aib)$_4$-OMe are similar. This suggests that the amino acid type plays a significant role in determining the secondary structure of L/D-peptides, even when the peptide contains Aib as a helical inducer. Based on these observations, we concluded that peptides **2** and **3** formed random coil structures in aqueous solution.

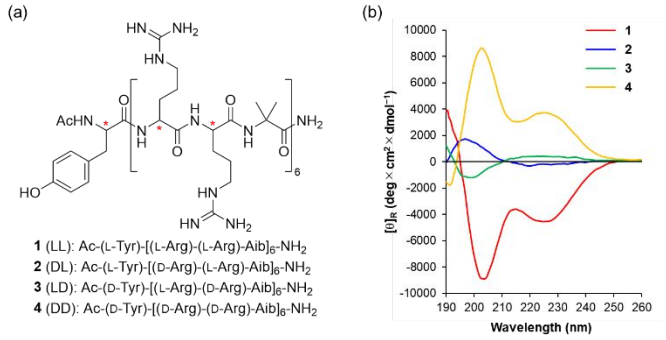

Figure 2. (a) Chemical structures of peptides **1**–**4**. (b) CD spectra of **1**–**4** in water (0.05 mM).

Peptide stability.

To quantify the stability of the peptides against enzymes, the enzymatic resistance of peptides was evaluated by treating them with pronase, a nonspecific protease mixture derived from the culture supernatant of *Streptomyces griseus* (Figure 3). In this experiment, R9 was used for comparison. Peptides were incubated with pronase (0.0005 w/v%) for 15, 30, 60, and 120 min at 37 °C, and rate of degradation of peptide was assessed by monitoring the LC-MS. The R9 peptide was rapidly degraded by pronase, with no intact peptide remaining after 120 min, whereas the incorporation of Aib enhanced the peptide stability, with approximately 20% of peptide **1** remaining intact after 120 min. This finding, that peptide stability is improved by incorporating Aib into CPPs, is consistent with the results reported in previous studies.[14] Furthermore, the dual modification of the peptides with D-amino acids and Aib significantly enhanced their enzyme resistance, with approximately 90% of the peptides remaining intact after 120 min.

Figure 3. Peptide stability against pronase (0.0005 w/v%) at various incubation times.

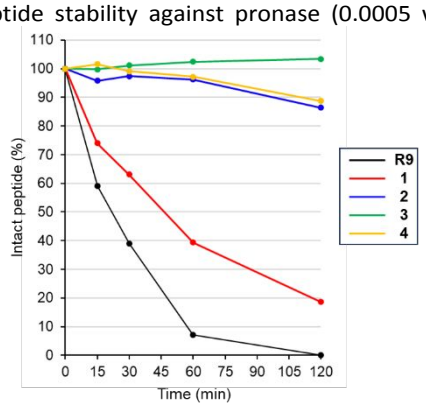

Physicochemical properties of peptide/pDNA complexes.

To evaluate the binding ability of each peptide to pDNA, we conducted agarose gel electrophoresis of the peptide/pDNA complexes at various N/P ratios, defined as the molar ratio of

guanidino groups (N) in the peptides to phosphate groups (P) in pDNA. The results indicated that even at an N/P ratio of 2, all the peptides successfully formed NPs with pDNA (Figure 4). Subsequently, we investigated the physicochemical properties of the peptide/pDNA complexes, including the particle size and zeta potential, to gain further insight into the characteristics of the formed NPs (Table 1). Most peptides, with the exception of peptide **4** at N/P = 2, formed NPs with sizes less than 300 nm and narrow polydispersity indexes (PDIs), which are suitable for intracellular internalization. Notably, the larger size and higher PDI of the NPs formed with peptide **4** at N/P = 2 suggested that these NPs may be relatively unstable. Peptides **2** and **3**, which contain L- and D-amino acids and form random coil structures, were significantly smaller than peptides **1** and **4**, which possess a single-handed chirality and form a single-handed helical structure. We assumed that the flexible conformations, such as random coil structures, of heterochiral peptides **2** and **3**, may facilitate the formation of complexes with pDNA. In addition, we observed a strong correlation between the size and zeta potential of the NPs, with smaller particles generally exhibiting a more positive charge. These findings suggest that pDNA recognizes the chirality or conformation of peptides and forms NPs in a somewhat different manner. The results of complex formation between pDNA and homo-/heterochiral peptides **1**–**4** are consistent with recent findings regarding the interactions between siRNA and homo-/heterochiral peptides.[15]

Figure 4. Gel retardation analysis of peptides **1**–**4**/pDNA

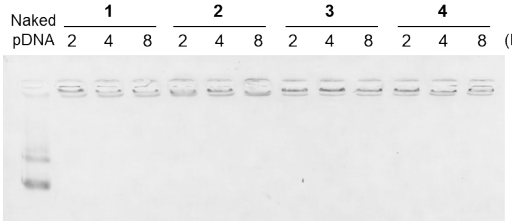

complexes prepared at N/P = 2, 4, and 8.

Table 1. Sizes, PDI, and zeta-potentials of the peptide/pDNA complexes prepared at N/P = 2, 4, and 8.

Peptide	N/P	Size (nm)	PDI (μ/Γ^{-2})	Zeta-potential (mV)
1	2	269 ± 5	0.114 ± 0.026	26.8 ± 0.9
	4	168 ± 1	0.103 ± 0.010	29.2 ± 0.3
	8	147 ± 1	0.148 ± 0.007	31.1 ± 0.7
2	2	201 ± 1	0.079 ± 0.011	29.0 ± 0.9
	4	136 ± 0	0.094 ± 0.009	29.6 ± 0.7
	8	130 ± 1	0.133 ± 0.015	33.6 ± 0.5
3	2	216 ± 1	0.083 ± 0.010	29.4 ± 0.4
	4	137 ± 0	0.077 ± 0.010	30.9 ± 0.2
	8	125 ± 1	0.091 ± 0.007	32.0 ± 0.8
4	2	566 ± 5	0.262 ± 0.005	25.2 ± 1.0
	4	164 ± 1	0.177 ± 0.013	28.5 ± 0.3
	8	139 ± 1	0.133 ± 0.003	31.5 ± 0.6

pDNA delivery using peptide/pDNA complexes.

Before assessing the transfection efficiency of the pDNA/peptide complexes, we evaluated the cytotoxicity of peptides **1**–**4** using a Cell Counting Kit-8 (CCK-8) and a lactate dehydrogenase (LDH) assay kit (Figure S1 and S2). Huh-7 cells were incubated with complexes of pDNA and peptides **1**–**4** along with jetPEI, a commercially available transfection reagent, at various N/P ratios for 24 h. While peptides **1**–**4** resulted in a minor dose-dependent reduction in cell proliferation, the cytotoxicity of jetPEI was significant (Figure S1). Similarly, the peptides demonstrated only a limited degree of membrane disruption compared with jetPEI (Figure S2). These findings suggested that Arg-rich peptides are safer than jetPEI. Furthermore, microscopic analysis showed no noticeable damage to the cells after a 24-hour treatment with the peptides (Figure S3). Subsequently, the transfection efficiency of the complexes at N/P ratios of 2, 4, and 8 were evaluated using the luciferase assay (Figure 5). Luciferase-encoding pDNA was complexed with peptides **1**–**4** and then subjected to Huh-7 cells for 24 h at 37 °C. Following removal of the complexes, the cells were incubated for an additional 24 and 48 h. JetPEI was used as a positive control at N/P = 8. Although distinct differences in transfection efficiency after 24-h of additional incubation were observed among the individual peptides at N/P = 2, similar results were obtained at N/P = 4 and 8, where the complexes formed NPs of < 200 nm in size (Figure 5a). At N/P = 2, the order of the transfection efficiency for the peptide/pDNA complexes was **4** < **1** ≤ **3** < **2**, which correlated well with the particle size of the NPs. Extending the incubation time to 48 h resulted in an enhanced luminescence at N/P = 2; however, no significant changes were observed at N/P = 4 or 8 (Figure 5b). We expected that substituting L-amino acids with D-isomers would facilitate long-term uptake owing to their increased stability. However, a slight reduction in the luminescence was observed for the peptides containing D-isomers, whereas peptide **1** exhibited a slight enhancement in luminescence. For pDNA to function, it must be released from NPs after cellular uptake. Peptides containing D-amino acids may be disadvantageous in this step because of their exceptionally high stability (Figure 3).

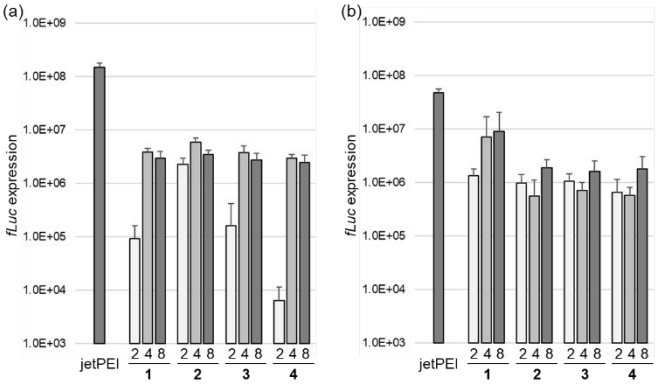

Figure 5. Transfection efficiencies of pDNA using peptides **1**–**4** (N/P = 2, 4, and 8) and jetPEI (N/P = 8) after (a) 24-hours and (b) 48-hours additional incubation. Error bars represent the standard deviation (n = 5).

Cellular uptake of peptide/pDNA complexes.

The cellular uptake of Cy5-labeled pDNA (Cy5-pDNA) complexed with each peptide was quantified using flow cytometry (Figure 6a). Huh-7 cells were incubated with peptide/Cy5-pDNA complexes at N/P ratios of 2, 4, and 8 for 24 h, and uptake was evaluated. Among all the peptides, lower fluorescence intensities were observed at N/P = 2. Notably, the cellular uptake of Cy5-pDNA was relatively lower for peptide **4** at N/P = 4 than for the other peptides, although the transfection efficiencies were not significantly different from those of the other peptides (Figure 4). We speculated that the peptide **4**/pDNA complexes were more effective at escaping the endosome, as D-peptides were more prone to endosomal escape than their L-counterparts.[15,16] To further investigate the behavior of the peptide/Cy5-pDNA complexes within cells, super-resolution fluorescence microscopy was performed (Figure 6b). Huh-7 cells were incubated with peptide **1**–**4**/Cy5-pDNA complexes at N/P = 8 and co-stained with LysoTracker Green and Hoechst33342 to stain the lysosomes and nuclei, respectively. No significant differences were observed between the individual peptides. Therefore, another underlying factor may explain the discrepancy between the transfection efficiency and cellular uptake efficiency of D-CPP **4**.

Figure 6. (a) Cellular uptake of Cy5-pDNA delivered by **1**–**4**. Error

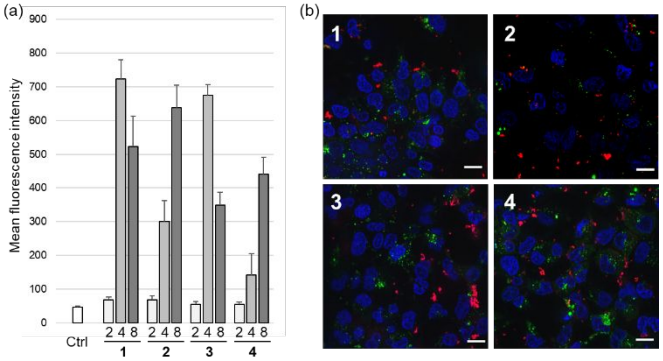

bars represent the standard deviation (n = 3). (b) Super-resolution fluorescence microscopic observations of Cy5-pDNA (red) delivered by peptides **1**–**4** at N/P ratio = 8. Blue: nuclei (Hoechst 33342). Green: late-endosome and lysosome (LysoTracker Green). The scale bars represent 20 μm.

Conclusions

In conclusion, we developed arginine-rich CPPs composed of L- and D-amino acids, along with Aib, for efficient intracellular pDNA delivery. Aib, known for its ability to induce helical structures, caused homochiral peptides **1** and **4** to adopt (*P*) and (*M*) helices, as observed in the CD spectra, whereas heterochiral peptides **2** and **3** did not form typical single-handed helical structures. This conformational difference may have partially influenced the formation of NPs with pDNA and their transfection efficiency. In pDNA transfection experiments using CPP/pDNA complexes, the particle size and zeta potential at low N/P ratios were influenced by the configuration of the amino acids, leading to varying pDNA delivery efficiencies for each peptide. However, at higher N/P ratios, no significant differences were observed among the peptides despite clear differences in their enzyme stability depending on whether they contained D-amino acids. As a result, helical CPP foldamer **1** gave slightly better results than the others. The efficiency of pDNA delivery through non-covalent interactions may be influenced by factors beyond the stability and membrane permeability of the peptide itself, such as the release efficiency of pDNA from NPs, which could be affected by the rigidity of the CPP/pDNA complexes.

Experimental

General information.

Peptides were prepared automatically using the Biotage peptide synthesizer Syro I (Biotage Japan, Tokyo, Japan). The LC-MS spectra were recorded using an Agilent 6230B TOF mass spectrometer (Agilent Technologies Inc., U.S.A.). All reagents and solvents were of commercial grade and used as supplied, unless otherwise noted. pDNA encoding luciferase (Luc) under the control of the CAG promoter was obtained from the RIKEN Gene Bank (Tsukuba, Japan). Dulbecco's modified Eagle's medium (DMEM) was purchased from Sigma-Aldrich (St. Louis, MO, U.S.A.). Luciferase assay kit was purchased from Promega (Madison, WI, U.S.A.). pDNA was labeled with Cy5 (Cy5-pDNA) using the Label IT® Tracker™ intracellular Nucleic Acid Localization Kit obtained from Mirus Bio Co. (Madison, WI, U.S.A.). Cell Counting Kit-8, LDH assay kit, Hoechst 33342 and LysoTracker Green DND-26 were purchased from Dojindo Laboratories (Kumamoto, Japan) and Molecular Probes (Eugene, OR), respectively.

Peptide synthesis.

The Rink Amide Protide resin (0.20 mmol/g capacity, CEM Corp. Matthews, NC, U.S.A.) was swelled in CH_2Cl_2 for 2 h. After removal of CH_2Cl_2, peptides were synthesized using Fmoc-amino acids (3 equiv), 1-[bis(dimethylamino)methylene]-1*H*-1,2,3-triazolo[4,5-*b*]pyridinium 3-oxide hexafluorophosphate (HATU; 3 equiv), 3*H*-[1,2,3]triazolo[4,5-*b*]pyridin-3-ol (HOAt; 3 equiv), and *N*,*N*'-diisopropylethylamine (6 equiv) as coupling reagents. Unreacted *N*-terminal amines were capped with acetic anhydride after each coupling step. Upon completion of the desired sequence, a cleavage cocktail (95% trifluoroacetic acid [TFA], 2.5% water, and 2.5% triisopropylsilane) was added to the resin at 0 °C, and the mixture was allowed to stand for 90 min. After removing TFA under a stream of N_2, cold diethyl ether was added to precipitate the peptides. The dried crude peptides were dissolved in water and purified using reverse-phase HPLC. After purification, the peptide solution was lyophilized. Peptide purity was assessed using analytical HPLC with an InertSustainSwift C18 column (5 μm, 4.4 mm × 250 mm; solvent A: 0.1% TFA/water; solvent B: 0.1% TFA/MeCN; flow rate: 1.0 mL/min, gradient: 5–95% solvent B over 30 min).

CD spectral measurements.

CD spectra were recorded using a JASCO CD spectrometer with a 1.0 mm path length cell. The peptides were dissolved in ultrapure water at a concentration of 50 μM, and spectra were acquired over a wavelength range of 260–190 nm.

Resistance to proteases.

Peptides and pronase were mixed in phosphate buffered saline (PBS) to final concentrations of 50 μM and 5 × 10^{-4} w/v%, respectively, and incubated at 37 °C for 0, 15, 30, 60, or 120 min. After each incubation period, 75 μL of the mixture was aliquoted, and 75 μL of 1% TFA/PBS solution was added to inactivate the pronase. Peptide stability was evaluated by LC-MS.

Agarose gel electrophoresis.

The gel electrophoresis was conducted at 100 V for 30 min on a 1% agarose gel. Subsequently, the pDNA was stained with SYBR Gold and visualized using the GelDoc Go Gel Imaging System (Bio-Rad Laboratories, Inc., Hercules, CA, U.S.A.).

Dynamic light scattering (DLS) measurements.

The size of the nanoparticles formed from peptide/pDNA complexes was determined by DLS. All measurement were recorded using a Nano ZS instrument (ZEN3600, Malvern Instruments, Ltd., U.K.). A He-Ne ion laser (633 nm) was used as the incident beam. Light scattering data were collected at a detection angle of 173° and at a temperature of 25 °C and were analyzed using the cumulant method to calculate the hydrodynamic diameters and polydispersity index (PDI) (μ/Γ^{-2}) of the complexes. Results are presented as the mean and standard deviation of three measurements.

Zeta-potential measurements.

The zeta potentials of the nanoparticles formed from peptide/pDNA complexes were evaluated using laser Doppler electrophoresis with a Nano ZS instrument equipped with a He-Ne ion laser (633 nm). Zeta-potential measurements were conducted at 25 °C, with a scattering angle of 173°. The results are presented as the mean and standard deviation derived from three measurements.

Cell viability assay.

Huh-7 cells were seeded onto 96 wells plates (5,000 cells/well) in 100 μL of DMEM containing 10% fetal bovine serum (FBS) and 1% penicillin/streptomycin (PS) and incubated overnight at 37 °C. The culture medium was then replaced with fresh medium, and peptide/pDNA complex solutions at various N/P ratios were added, ensuring a final concentration of 0.25 μg of pDNA per well. After 24 h of incubation, cell viability was assessed using Cell Counting Kit-8, following the manufacturer's protocol. The results are presented as the mean and standard error of the mean obtained from four samples.

Lactate dehydrogenase (LDH) assay.

Huh-7 cells were seeded onto 96 wells plates (5,000 cells/well) in 100 μL of DMEM containing 10% FBS and 1% PS, and incubated overnight at 37 °C. The culture medium was then exchanged with fresh medium, and peptide/pDNA complex solutions at various N/P ratios were added to achieve a final concentration of 0.25 μg pDNA per well. After 24 h of incubation, the LDH activity was evaluated using an LDH assay kit according to the manufacturer's protocol. The results are presented as the mean and standard error of the mean obtained from four samples.

pDNA transfection assay.

Huh-7 cells were seeded onto 96 wells plates (5,000 cells/well) in 100 μL of DMEM containing 10% FBS and 1% PS and incubated overnight at 37 °C. The culture medium was then exchanged with fresh medium, and peptide/pDNA complex solutions at various N/P ratios were added to achieve a final concentration of 0.25 μg pDNA per well. After 24 h of incubation, the medium was replaced with fresh culture medium and incubation was continued for an additional period. After 24 or 48 h, Luc gene expression was assessed by measuring photoluminescence intensity using a luciferase assay kit and a Lumat3 LB9508 luminometer (Berthold Technologies, Bad Wildbad, Germany). The results are presented as the mean and standard error of the mean obtained from five samples.

Cellular uptake.

Huh-7 cells were seeded onto 24 wells plates (50,000 cells/well) in 500 μL of DMEM containing 10% FBS and 1% PS, and incubated overnight at 37 °C. The culture medium was then replaced with fresh medium and peptide/Cy5-pDNA complex solutions at various N/P ratios were added to achieve a final concentration of 1 μg pDNA per well. After 24 h of incubation, the medium was removed and the cells were washed with ice-cold PBS three times and trypsinized. After dilution with PBS, the fluorescence intensity of the collected cells was measured by flow cytometry using a Guava Muse (Cytek Biosciences, Amsterdam, Netherlands). The results are presented as mean and standard error of the mean obtained from three samples.

Super-resolution fluorescence microscopic observation.

Huh-7 cells were cultured at a density of 20,000 cells per well in glass-bottom dishes (35 mm) in 200 μL of DMEM containing 10% FBS and 1% PS and incubated overnight at 37 °C. The culture medium was then replaced with fresh medium, and peptide/Cy5-pDNA complex solutions at N/P = 8 were added to achieve a final concentration of 0.33 μg pDNA per well. After 24 h of incubation, the medium was removed, and the cells were washed three times with PBS. The cells were co-stained with Hoechst 33342 and LysoTracker Green following the manufacturer's protocol and observed using a BZ-X800 (KEYENCE CORPORATION, Osaka, Japan). For Hoechst 33342, λ_{ex} = 360 nm, λ_{em} = 435–485 nm. For LysoTracker, λ_{ex} = 470 nm, λ_{em} = 500–550 nm. For Cy5, λ_{ex} = 620 nm, λ_{em} = 662.5–737.5 nm.

Author contributions

Conceptualization and funding acquisition: T.U. and M.O.; Methodology, investigation, analysis, and writing–original draft preparation: T.U.; Writing–review and editing: H.T. and M.O.; Supervision and project administration: M.O. All authors have read and agreed to the published version of the manuscript.

Conflicts of interest

There are no conflicts to declare.

Data availability

The data supporting this article have been included as part of the Supplementary Information.

Acknowledgements

This work was supported by a Grant-in-Aid for Early-Career Scientists (Grant Number 22K15265 for T.U.), the Japan Society for Promotion Sciences (JSPS), and the Japan Science and Technology Agency COI-NEXT (Grant Number JPMJPF2114 for M.O.). We thank C. Takayama and S. Ibuki for technical assistance.

References

1 (a) H. Derakhshankhah and S. Jafari, *Biomed. Pharmacother.*, 2018, **108**, 1090–1096. (b) M. Oba, *ChemBioChem*, 2019, **20**, 2041–2045. (c) K. Desale, K. Kuche and S. Jain, *Biomater. Sci.*, 2021, **9**, 1153–1188.

2 (a) T. Takeuchi and S. Futaki, *Chem. Pharm. Bull.*, 2016, **64**, 1431–1437. (b) I. Ruseska and A. Zimmer, *Beilstein J. Nanotechnol.*, 2020, **11**, 101–123. (c) A. Gori, G. Lodigiani, S. G. Colombarolli, G. Bergamaschi and A. Vitali, *ChemMedChem*, 2023, **18**, e202300236.

3 G. C. Kim, D. H. Cheon and Y. Lee, *Biochim. Biophys. Acta (BBA)-Prot. Proteom.*, 2021, **1869**, 140604.

4 (a) S.-i. Wada, Y. Hirota, R. Tanaka and H. Urata, *Bioorg. Med. Chem. Lett.*, 2008, **18**, 3999−4001. (b) M. Oba, M. Kunitake, T. Kato, A. Ueda and M. Tanaka, *Bioconjugate Chem.*, 2017, **28**, 1801–1806. (c) M. Oba, Y. Nagano, T. Kato and M. Tanaka, *Sci. Rep.*, 2019, **9**, 1349. (d) M. Oba, S. Nakajima, K. Misao, H. Yokoo and M. Tanaka, *Bioorg. Med. Chem.*, 2023, **91**, 117409.

5 (a) G. Tünnemann, G. Ter-Avetisyan, R. M. Martin, M. Stöckl, A. Herrmann and M. C. Cardoso, *J. Pept. Sci.*, 2008, **14**, 469–476. (b) P. A. Wender, D. J. Mitchell, K. Pattabiraman, E. T. Pelkey, L. Steinman and J. B. Rothbard, *Proc. Natl. Acad. Sci. U.S.A.*, 2000, **97**, 13003–13008. (c) A. Elmquist and Ü. Langel, *Biol. Chem.*, 2003, **384**, 387–393. (d) S. Pujals, J. Fernández-Carneado, M. D. Ludevid and E. Giralt, *ChemMedChem*, 2008, **3**, 296–301.

6 W. P. R. Verdurmen, P. H. Bovee-Geurts, P. Wadhwani, A. S. Ulrich, M. Hällbrink, T. H. van Kuppevelt and R. Brock, *Chem. Biol.*, 2011, **18**, 1000–1010.

7 (a) H. Yamashita, Y. Demizu, T. Shoda, Y. Sato, M. Oba, M. Tanaka and M. Kurihara, *Bioorg. Med. Chem.*, 2014, **22**, 2403–2408. (b) H. Takada, K. Tsuchiya and Y. Demizu, *Bioconjugate Chem.*, 2022, **33**, 1311–1318. (c) M. Hirano, H. Yokoo, N. Ohoka, T. Ito, T. Misawa, M. Oba, T. Inoue and Y. Demizu, *Chem. Pharm. Bull.*, 2024, **72**, 149–154.

8 (a) I. L. Karle and P. Balaram, *Biochemistry*, 1990, **29**, 6747–6756. (b) H. Heimgartner, *Angew. Chem., Int. Ed.*, 1991, **30**, 238–264.

9 M. Oba, Y. Ito, T. Umeno, T. Kato and M. Tanaka, *ACS Biomater. Sci. Eng.*, 2019, **5**, 5660−5668.

10 G. Holzwarth and P. Doty, *J. Am. Chem. Soc.*, 1965, **87**, 218–228.

11 (a) C. Toniolo and E. Benedetti, *Maclomolecules*, 1991, **24**, 4004−4009. (b) H. Yokoo, A. Dirisala, S. Uchida and M. Oba, *ACS Biomater. Sci. Eng.*, 2024, **10**, 890−896.

12 T. Misawa, N. Ohoka, M. Oba, H. Yamashita, M. Tanaka, M. Naito and Y. Demizu, *Chem. Commun.*, 2019, **55**, 7792−7795.

13 Y. Demizu, H. Yamashita, N. Yamazaki, Y. Sato, M. Doi, M. Tanaka and M. Kurihara, *J. Org. Chem.*, 2013, **78**, 12106−12113.

14 (a) S. Zikou, A.-I. Koukkou, P. Mastora, M. Sakarellos-Daitsiotis, C. Sakarellos, C. Drainas and E. Panou-Pomonis, *J. Pept. Sci.*, 2007, **13**, 481–486. (b) I. Tarasenko, N. Zashikhina, I. Guryanov, M. Volokitina, B. Biondi, S. Fiorucci, F. Formaggio, T. Tennikova and E. Korzhikova-Vlakh, *RSC Adv.*, 2018, **8**, 34603–34613. (c) C. Peggion, V. Panetta, L. Lastella, F. Formaggio, A. Ricci, S. Oancea, G. Hilma and B. Biondi, *J. Pept. Sci.*, 2024, **30**, e3609.

15 Z. Wang, L. Yue, J. Min, H. Liu, Y. Zhang, Y. Du, R. Su, W. Qi and Y. Wang, *Nano Lett.*, 2025, **25**, 2693−2701.

16 K. Najjar, A. Erazo-Oliveras, D. J. Brock, T.-Y. Wang and J.-P. Pellois, *J. Biol. Chem.*, 2017, **292**, 847–861.

Data availability

The data supporting this article have been included as part of the Supplementary Information.